

Search for Large Extra Dimensions Using Dielectron and Diphoton Events in $p\bar{p}$ Collisions at $\sqrt{s} = 1.8$ TeV

David Gerdes^a, Simona Murgia^{c,d}, John Carlson^a, Robert E. Blair^b, Joey Houston^c, Daniel Berebitsky^a

^a *Department of Physics, University of Michigan, Ann Arbor, MI 48109*

^b *HEP Division, Argonne National Laboratory, Argonne, IL 60439*

^c *Department of Physics and Astronomy, Michigan State University, East Lansing, MI 48824*

^d *Department of Physics, Stanford University, Stanford, CA 94305*

(Dated: November 23, 2018)

Arkani-Hamed, Dimopoulos, and Dvali have proposed a model of low-scale quantum gravity featuring large extra dimensions. In this model, the exchange of Kaluza-Klein towers of gravitons can enhance the production rate of electron and photon pairs at high invariant mass in proton-antiproton collisions. The amount of enhancement is characterized by the parameter M_S , the fundamental Planck scale in the bulk extra dimensions. We have searched for this effect using 100 pb⁻¹ of diphoton data and 110 pb⁻¹ of dielectron data collected with the Collider Detector at Fermilab at $\sqrt{s} = 1.8$ TeV during the 1992-1996 run. In the absence of a signal, we place 95% confidence-level limits on M_S of 905 GeV/ c^2 and 826 GeV/ c^2 , for the case of constructive and destructive graviton interference respectively.

PACS numbers: 04.50.+h, 04.80.Cc, 13.85.Qk, 13.85.Rm

Theories of low-scale quantum gravity featuring large extra spatial dimensions (LED) have attracted considerable interest because of their possible observable consequences at existing and future colliders. In one such scenario, proposed by Arkani-Hamed, Dimopoulos, and Dvali [1], the fermions and gauge bosons of the Standard Model (SM) are confined to the three ordinary spatial dimensions, which form the boundary (“the brane”) of a space with n compact spatial dimensions (“the bulk”) in which gravitons alone can propagate. In this model, the Planck scale is lowered to the electroweak scale of $\mathcal{O}(1$ TeV), which is postulated to be the only fundamental scale in nature. The fundamental Planck scale in the extra dimensions (M_S), the characteristic size of the n extra dimensions (R) and the Planck scale on the brane (M_{Pl}) are related via

$$M_{Pl}^2 \propto M_S^{n+2} R^n, \quad (1)$$

a purely classical relationship calculated by applying the $4 + n$ dimensional Gauss’s law. In this scenario, then, the weakness of gravity compared to the other SM interactions is explained by the suppression of the gravitational field flux by a factor proportional to the volume of the extra dimensions.

One important consequence for physics in the brane is that the discrete momentum modes of excitation of the graviton transverse to the brane propagate in our three ordinary dimensions as different mass states. Analogously to the momentum states, the spacing between these mass states is proportional to $1/R$. This collection of mass states forms what is known as a Kaluza-Klein (KK) tower of gravitons. The tower can in principle extend up to infinity, but there is a cutoff imposed by the fact the effective theory breaks down at scales above M_S .

The existence of KK gravitons can be tested at colliders by searching for two different processes: real graviton emission and virtual graviton exchange. At leading order, virtual graviton exchange includes processes in which a virtual graviton is produced by the annihilation of two SM particles in the initial state, the graviton then propagates in the extra dimension and finally decays into SM particles that appear in the brane. Real graviton production occurs when a graviton is produced together with something else by the interaction of SM particles and escapes into the extra dimensions, leaving behind missing energy.

In this paper, we search for LED by looking for the decay of KK gravitons into diphotons [2] or dielectrons [3]. An analysis of these final states has previously been carried out by the DØ Collaboration [4]. These channels are desirable because SM production of these pairs involves an electromagnetic coupling to the final state; thus production is suppressed with respect to dijet final states. However, gravitons couple democratically to stress-energy. Thus, LED production of dielectron and diphoton final states can more easily be distinguished from SM sources. The dominant Feynman diagrams that contribute to these processes in the SM are shown in Figure 1. When KK gravitons are included, new diagrams appear as shown in Figure 2. Since the LED contribution to SM pair production proceeds through a KK tower of graviton states with a closely spaced mass spectrum, the extra-dimensional signal does not appear as a single resonance, but rather as an enhancement of the production

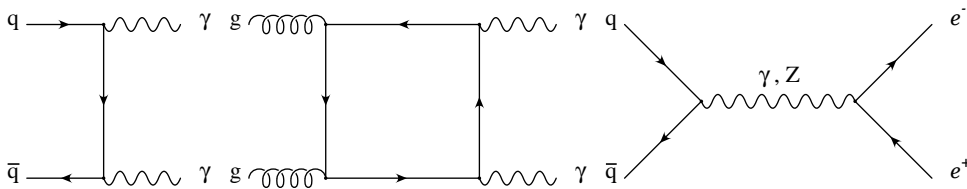


FIG. 1: Feynman diagrams for SM diphoton and dielectron production at leading order.

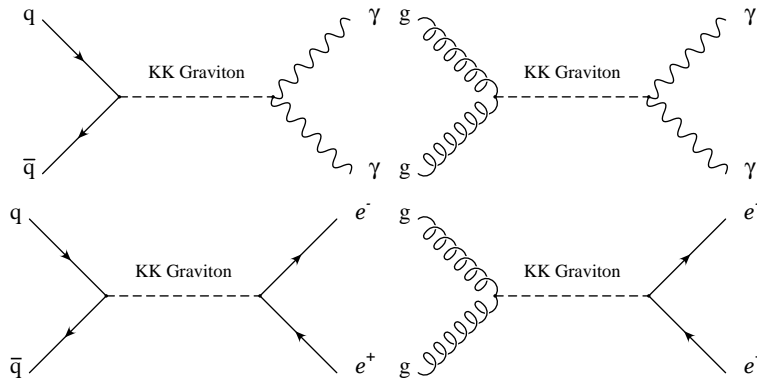


FIG. 2: Feynman diagrams for LED diphoton and dielectron production at leading order.

cross section at high invariant mass where the SM contribution is rapidly falling and a large number of gravitons can be produced or, equivalently, more modes of the momentum in the bulk can be excited.

The cross section for graviton production at leading order, as a function of the invariant mass of the electron or photon pair, takes the general form [5]:

$$\frac{d\sigma}{dM} = f_{SM}(M) + \eta_{LED} f_{INT}(M) + \eta_{LED}^2 f_{KK}(M), \quad (2)$$

where M is the invariant mass of the photon or electron pair and f_{SM} , f_{INT} , f_{KK} are terms in the cross section with the dimensionful parameter η_{LED} factored out. The term f_{SM} on the right-hand side of Equation 2 is the contribution from SM processes only. The second term, f_{INT} , proportional to the first power of η_{LED} , is the result of the interference between the SM and the LED graphs. Finally, the last term, f_{KK} , proportional to η_{LED}^2 , is the contribution coming from the direct KK tower exchange. Graviton-mediated processes introduce the η_{LED} -dependence in the equation, where $\eta_{LED} = \lambda/M_S^4$ is the parameter that characterizes LED: M_S represents the Planck scale in the bulk and should be of order 1 TeV and λ is a dimensionless parameter of $\mathcal{O}(1)$ and its value is model-dependent. The different signs of λ allow for different signs of the interference between SM and LED graphs. The shapes of the interference and direct KK cross sections are independent of η_{LED} , which affects only the relative and absolute normalization, while the shapes themselves depend only on the parton distribution functions (PDF's) and the kinematics of the process.

As an illustration, Figure 3 shows the diphoton invariant mass spectrum for the case $M_S = 750 \text{ GeV}/c^2$ with constructive interference between the SM and LED diagrams. The LED signal clearly stands out above the background at higher values of the invariant mass. The signal in the dielectron case is similar. We have searched for this signal in approximately 110 pb^{-1} of data collected in proton-antiproton collisions at $\sqrt{s} = 1.8 \text{ TeV}$ by the Collider Detector at Fermilab (CDF) experiment during the 1992-96 run (Run I).

The Run I CDF detector has been described in detail in Reference [6]. Here we present an overview of the detector components most relevant to this analysis. The central portion of the detector is cylindrically symmetric around the beam pipe. Forward/backward extensions together with the central section of the detector provide close to 4π coverage of the solid angle. Three tracking systems (SVX, VTX, CTC), situated inside a 1.4 T superconducting solenoid, allow measurements of charged particle momenta for pseudorapidity $|\eta| < 1.1$. In addition, the SVX allows measurement of secondary vertices and the VTX provides information on the location of the primary vertex along the beam axis. Located right outside the solenoid coil, the Central Preradiator (CPR), a multi-wire proportional drift chamber, measures tracks of charged particles that result from photon conversions in the inner detector. The electromagnetic (EM) and hadronic calorimeter systems are also located outside the solenoid coil, past the CPR. They consist of sampling devices with alternating layers of sensitive

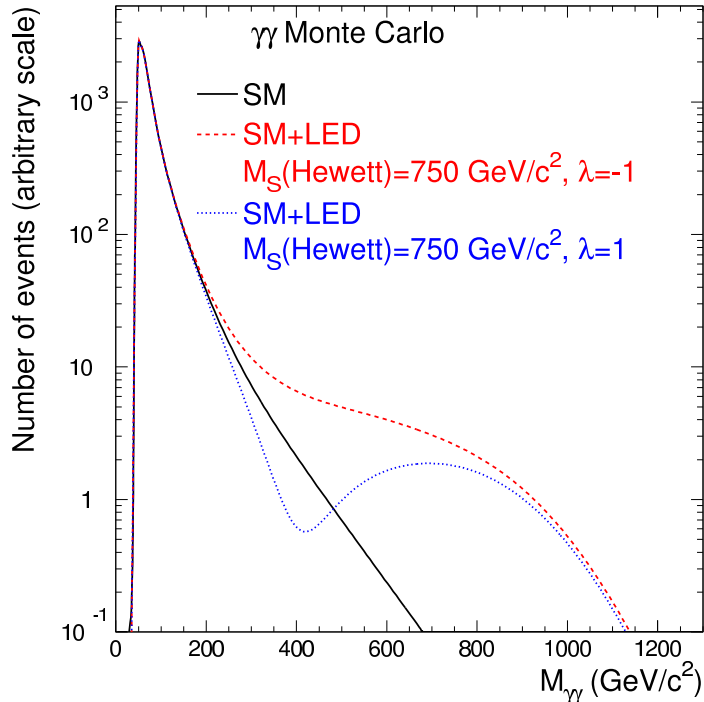


FIG. 3: An example of LED ($M_S = 750 \text{ GeV}/c^2$) contributions is shown along with the SM prediction in the diphoton invariant mass distribution. The two curves for LED are for constructive ($\lambda = -1$) and destructive ($\lambda = +1$) interference with the SM processes.

and absorbing materials, and are segmented in η, ϕ towers with projective geometry. The calorimeter is divided into three components covering different regions of pseudorapidity: central ($|\eta| < 1.1$), end-plug ($1.1 < |\eta| < 2.4$) and forward ($2.4 < |\eta| < 4.2$). Only the central and end-plug regions are used in this analysis. The central strip chambers (CES) are embedded into the central EM calorimeter section, and provide a high-resolution measurement of the lateral shower profile in z and $r - \phi$ at the point of its maximum development. Finally, muon chambers are located outside the calorimeter to detect particles that escape the inner layers of the detector.

The diphoton sample consists of two distinct subsets, corresponding to two different event topologies. One of the subsets, the Central-Central (CC) diphoton sample, consists of events with both photons in the central region of the detector, while the other, the Central-Plug (CP) diphoton sample, has events with at least one central electromagnetic cluster and at least one cluster in the end-plug electromagnetic calorimeter. The CC diphoton sample has been described in Reference [7]. Photons in this sample are required to have transverse energy (E_T) $> 22 \text{ GeV}$, to pass a calorimeter isolation cut, to have no nearby charged tracks, and to have a CES shower profile consistent with that of a photon. The identification efficiency of the CC diphoton selection is 0.626 ± 0.017 , and the integrated luminosity of this sample is 100 pb^{-1} . A total of 287 CC events pass these cuts.

Two trigger paths are used to select the CP diphoton sample. The first path requires at least one isolated central EM cluster with $E_T > 23 \text{ GeV}$, while the second path requires an $E_T > 50 \text{ GeV}$ central EM cluster with no calorimeter isolation requirement. The central cluster must pass the the same offline selection applied to the CC diphoton sample but with an $E_T > 25 \text{ GeV}$ to ensure a high trigger efficiency. The plug EM cluster is required to have $E_T > 22 \text{ GeV}$. CTC tracking does not extend to the plug region of the detector; thus to reject charged particles we require that the fraction of hit wires in the VTX in a road centered on the cluster direction is smaller than 0.4. We require the E_T in the annulus between 0.4 and 0.7 in $\eta - \phi$ space around the cluster to be no larger than 4 GeV. This requirement allows us to select isolated clusters while avoiding possible inefficiency due to additional leakage into the cone immediately surrounding the cluster that occurs at larger rapidities. The efficiency of this cut is calculated with electrons from a $Z \rightarrow e^+e^-$ control sample, and is found to be 89%, 10% more than the canonical isolation cut based on a cone of 0.4. The identification efficiency of the CP diphoton selection is 0.550 ± 0.065 . In our integrated luminosity of 87 pb^{-1} , 192 CP events pass our cuts.

Dielectron events used in this analysis are required to have at least one “tight” electron candidate in the central calorimeter, while the second “loose” candidate can be in either the central or plug calorimeter. The

details of the selection requirements are described in References [3, 8]. All events must pass a central electron trigger that requires an EM cluster with $E_T > 22$ GeV together with a track with $p_T > 13$ GeV/ c . Offline, the tight electron must pass an E_T cut of 25 GeV and have the ratio of energy to momentum (E/p) < 4 . For tracks with $p_T > 50$ GeV/ c , no E/p cut is imposed. We require good agreement between the EM shower location and the extrapolated track position, and require the ratio of hadronic to electromagnetic energy in the cluster to be low. Finally, we require the electron to be isolated. The loose EM cluster is also required to have $E_T > 25$ GeV, but central candidates may pass more relaxed isolation and hadronic energy cuts. Plug electron candidates are required to have a low hadronic energy fraction, to be isolated, and to have a lateral shower profile consistent with that of testbeam electrons. The efficiency of the electron identification cuts is measured using Z data and is found to be 0.916 ± 0.010 for plug electrons and 0.961 ± 0.024 for central electrons. In an integrated luminosity of 110 pb^{-1} , we identify 3319 CC and 3825 CP candidates.

Both diphoton and dielectron events are generated using a leading-order matrix-element Monte Carlo (MC) program [9]. The simulation includes the matrix elements for direct SM diphoton production with $q\bar{q}$ or gg in the initial state, production via KK exchange from a $q\bar{q}$ or gg initial state, as well as interference between the SM and LED diphoton production processes with $q\bar{q}$ in the initial state. However, it does not include the interference between the gg -initiated SM and LED initial states, which is expected to be small [10]. A conservative estimate of this contribution is incorporated into the systematic uncertainties. The simulation also generates SM $q\bar{q} \rightarrow e^+e^-$ and $q\bar{q}$ or $gg \rightarrow e^+e^-$ events mediated by a KK tower of gravitons. The PYTHIA MC program [11] is used to model fragmentation, parton showers, and the underlying event with CTEQ5M PDF's [15]. The generated events are passed through a fast simulation of the CDF detector. We select simulated events using the same cuts applied to the data. This procedure yields a prediction of 96 ± 31 prompt SM diphoton events in the CC sample and 76 ± 14 events in the CP sample. In the dielectron sample, the prediction is 3463 ± 223 CC and 3883 ± 292 CP prompt SM dielectron events.

However, the bulk of the diphoton sample consists of events in which one or both electromagnetic clusters originate from jets. Hard jet fragmentation to leading neutral mesons (π^0, η) that subsequently decay into multiple photons can fake the prompt photon signature. In the CC case, the fake background is evaluated by employing statistical methods [12] that use CES and CPR pulse shape and height information to discriminate between prompt photons and photons originating from neutral meson decays. These techniques yield a fake estimate of $64 \pm 11 \pm 19\%$, which corresponds to $183 \pm 56 \pm 32$ events. The mass spectrum of the CC fake background is determined from the invariant mass distribution of events in a control sample of non-isolated diphotons [7].

In the CP case, we rely on the above techniques to determine the probability that the central cluster is a jet. However, these methods cannot be used for plug clusters. Instead, we employ dijet and non-isolated diphoton control samples to estimate the fake rate of events in which the central cluster is a prompt photon while the plug cluster is a jet [2]. The total number of fake events in the CP sample is 132 ± 31 . The mass spectrum of the CP fake background is determined by simulating SM γ +jet processes using the PYTHIA MC program and the CDF detector simulation. These events provide the mass spectrum for γ +fake events. The mass spectrum for events where both clusters are fakes is obtained by multiplying the MC γ +jet shape by the ratio between the $\pi^0\pi^0$ and $\gamma\pi^0$ cross sections calculated at leading order [13]. Because π^0 's are the main contribution to the fakes, we take this rescaled shape as the shape of the fake+fake contribution.

In summary, in the diphoton channel the prediction of fakes plus SM $\gamma\gamma$ is 280 ± 66 events in the CC sample and 208 ± 34 events in the CP sample, in good agreement with the observed 287 events in the CC case and 192 events in the CP case.

In the dielectron sample, the electrons in the final state are produced by other SM processes in addition to Drell-Yan. The dominant contribution is from QCD dijet events in which each jet contains a real or fake electron that survives the electron identification cuts. This mass distribution and size of this background is evaluated using samples of non-isolated dielectrons. We obtain 10 ± 6 background events in the CC case and 224 ± 17 background events in the CP case.

In summary, in the dielectron channel the number of events predicted, adding together background and SM contributions, is 3473 ± 223 CC and 4107 ± 293 CP dielectron events, in agreement with the observed 3319 events in the CC case and 3825 in the CP case.

We find that the data are in good agreement with the SM plus fakes prediction both with respect to the rate and invariant mass distribution. Figure 4 shows the data overlaid with the background predictions for diphoton and dielectron events. We therefore proceed to set a limit on LED by determining the lower bound on the parameter M_S that characterizes the strength of the graviton coupling. We do this by performing a likelihood fit to the diphoton and dielectron invariant mass distributions. We use two very similar likelihood functions, one for the diphoton and one for the dielectron case, which are multiplied together to obtain the overall likelihood function \mathcal{L} . The form of \mathcal{L} is similar to that employed in CDF's measurement of the top quark mass [14]. In the likelihood function, a Gaussian constraint is applied to the number of SM and fake dielectron and diphoton events in the CC and CP samples. In addition, a Poisson constraint is applied to the total number

of dielectron and diphoton events. Finally, a shape term weights the invariant mass of each event according to the consistency of its invariant mass with the SM, background, and LED shapes. We minimize $-\ln\mathcal{L}$ to obtain the best-fit value of $\eta_{LED} = \lambda/M_S^4$ for the cases $\lambda = \pm 1$, corresponding to constructive and destructive interference of the SM and KK terms. These values are consistent with zero, so we extract 95% confidence level (C.L.) limits. For the diphoton data alone, the limits on η_{LED} for constructive and destructive interference respectively are $\eta_{LED}=1.36 \text{ TeV}^{-4}$ and $\eta_{LED}=2.18 \text{ TeV}^{-4}$. For dielectrons, the limits are $\eta_{LED}=2.69 \text{ TeV}^{-4}$ (constructive) and $\eta_{LED}=2.86 \text{ TeV}^{-4}$ (destructive).

Systematic uncertainties in this analysis arise from effects that can modify the shapes of the SM, fake, and LED invariant mass distributions. In both the electron and photon analyses, the dominant effects are the choice of PDF's, variations in initial state radiation (ISR), and the shape of the CP fake background. Furthermore, the interference between SM and LED gg initial states is not included in the diphoton MC. To quantify these systematics, we generate shifted MC invariant mass distributions with each systematic effect separately varied. For example, we vary the choice of PDF's (CTEQ5HJ, MRST(h-g), MRST(larger d/u ratio), MRST(low- α_s), MRST(q_d), instead of the default CTEQ5M [15]), and turn off the effects of ISR. To estimate the uncertainty from the neglected gg interference term, we note that the cross section for the $gg \rightarrow \gamma\gamma$ process is about 30% of the $q\bar{q}$ process, so the gg interference term should be roughly $(0.3)^2 \approx 0.1$ of the $q\bar{q}$ one. We vary the $q\bar{q}$ interference portion of the templates by twice this amount, $\pm 20\%$. The systematic uncertainty on the CP background is estimated by using the second most populated region of the non-isolated dielectron control sample to determine the background shape, and computing the change in fitted η_{LED} versus the default (most populated region). For each systematic effect, many pseudo-experiments are generated at different values of M_S from the shifted distributions, and the resulting invariant mass distributions are fitted to our default templates. For each systematic effect, we determine the average shift between the input value of η_{LED} and the value extracted from the fit. The resulting shifts for all systematic effects are added in quadrature. The overall shift is used as the width of a gaussian that is convolved with the raw likelihood function from the fit to the data. Remaining uncertainties on efficiencies, acceptance, luminosity, and background normalization are already included in the width of the gaussian constraints in the likelihood function.

In the diphoton analysis, the 95% C.L. limits with systematics included are $\eta_{LED}=1.53 \text{ TeV}^{-4}$ (constructive interference) and $\eta_{LED}=2.48 \text{ TeV}^{-4}$ (destructive). In the dielectron case, we find $\eta_{LED}=2.70 \text{ TeV}^{-4}$ (constructive) and $\eta_{LED}=2.87 \text{ TeV}^{-4}$ (destructive).

Finally, we obtain the strongest limits by combining the diphoton and dielectron samples. A new fit is performed by multiplying the likelihood functions for each sample and minimizing it with respect to the common parameter η_{LED} . The systematic uncertainties are included into the combined limit in the following way. The full systematic uncertainties for the two search channels, $\Delta\eta_{LED,ee}(\eta_{LED})$ and $\Delta\eta_{LED,\gamma\gamma}(\eta_{LED})$, are broken into their component pieces, $\delta\eta_{LED,ee}^{PDF}$, $\delta\eta_{LED,ee}^{ISR}$, $\delta\eta_{LED,ee}^{uncorr}$, $\delta\eta_{LED,\gamma\gamma}^{PDF}$, $\delta\eta_{LED,\gamma\gamma}^{ISR}$ and $\delta\eta_{LED,\gamma\gamma}^{uncorr}$. Here $\delta\eta_{LED,ee}^{uncorr}$ represents the sum in quadrature of the dielectron systematics with the diphoton systematics, i.e. background and LED acceptance. Similarly, $\delta\eta_{LED,\gamma\gamma}^{uncorr}$ represents the sum in quadrature of the diphoton systematics uncorrelated with the dielectron systematics, i.e. SM+LED interference cross section and CP background. Each likelihood function, diphoton and dielectron, is smeared by taking the corresponding, unsmeared likelihood function, and smearing each point by throwing random numbers σ_i , $i=1,\dots,4$, and smearing a sample of values of η_{LED} in the following way:

$$\eta'_{LED,ee} = \eta_{LED,ee} + \sigma_1\delta\eta_{LED,ee}^{PDF}(\eta_{LED,ee}) + \sigma_2\delta\eta_{LED,ee}^{ISR}(\eta_{LED,ee}) + \sigma_3\delta\eta_{LED,ee}^{uncorr}(\eta_{LED,ee}) \quad (3)$$

$$\eta'_{LED,\gamma\gamma} = \eta_{LED,\gamma\gamma} + \sigma_1\delta\eta_{LED,\gamma\gamma}^{PDF}(\eta_{LED,\gamma\gamma}) + \sigma_2\delta\eta_{LED,\gamma\gamma}^{ISR}(\eta_{LED,\gamma\gamma}) + \sigma_4\delta\eta_{LED,\gamma\gamma}^{uncorr}(\eta_{LED,\gamma\gamma}). \quad (4)$$

This ensures that the uncorrelated uncertainties are smeared independently while the correlated PDF's and ISR uncertainties are smeared together.

After the smearing procedure is performed, the diphoton and dielectron smeared likelihood functions are multiplied together and the same method described above is used to calculate the combined dielectron-diphoton 95% C.L. limit on η_{LED} . We find $\eta_{LED}=1.49 \text{ TeV}^{-4}$ (constructive) and $\eta_{LED}=2.15 \text{ TeV}^{-4}$ (destructive).

The limits on η_{LED} are converted into limits on M_S by using the equation $\eta_{LED} = \lambda/M_S^4$. In Hewett convention [16], $\lambda = -1$ for constructive interference and $\lambda = +1$ for destructive interference. Other popular conventions are those of Giudice, Rattazzi, Wells (GRW) [17], and Han, Lykken, Zhang (HLZ) [18]. To translate results from Hewett to GRW convention one simply multiplies $M_S(\text{Hewett})$ by $\sqrt[4]{\pi/2}$ (constructive interference only). In HLZ convention the dependence on the number of extra dimensions n is calculated and it is incorporated into λ . For $n > 2$:

$$M_S(\text{HLZ}) = \sqrt[4]{\frac{\pi}{2} \left(\frac{2}{2-n} \right)} M_S(\text{Hewett}). \quad (5)$$

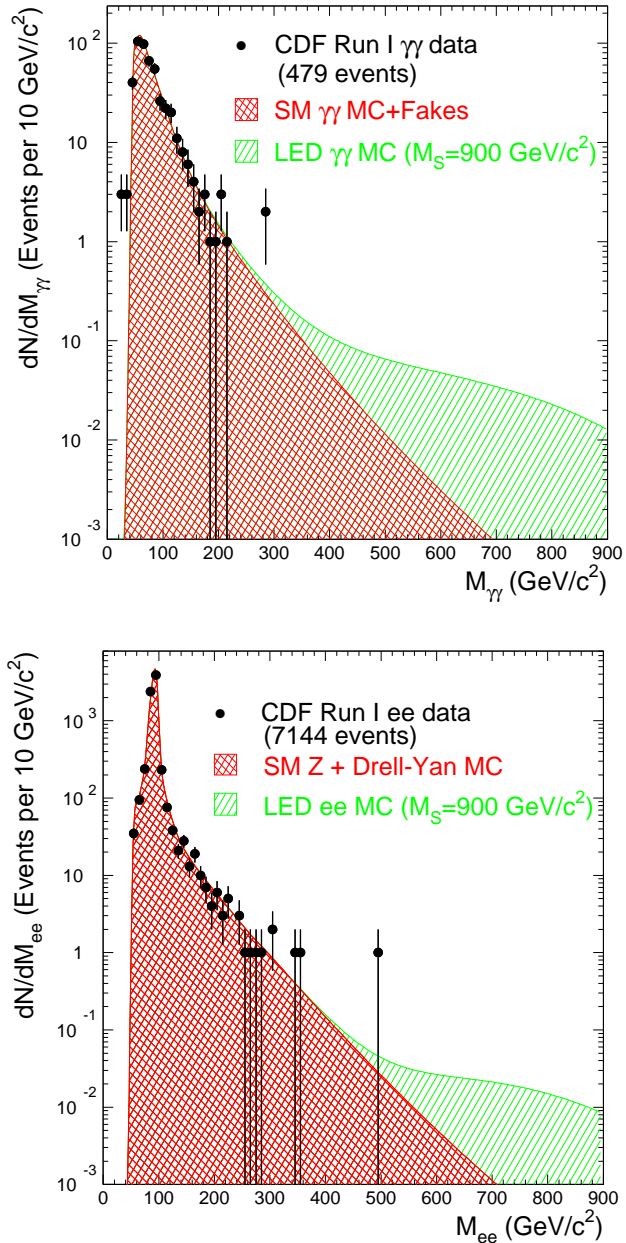


FIG. 4: Invariant mass distributions for the diphoton (top) and dielectron (bottom) data overlaid with the expected invariant mass distributions from SM and fake sources, as well as the LED contribution for $M_S(\text{Hewett}) = 900 \text{ GeV}/c^2$.

The dielectron and diphoton combined limits in these conventions are summarized in Table I. The limits quoted so far assume a K -factor of 1.0 for the LED process. Limits can be improved somewhat by assuming $K = 1.3$ to account for next-to-leading order effects for the SM diphoton and dielectron production as well as for the corresponding graviton mediated processes, as was done in Reference [4]. These limits are also shown in Table I.

We thank the Fermilab staff and the technical staffs of the participating institutions for their vital contributions. This work was supported by the U.S. Department of Energy and National Science Foundation; the Italian Istituto Nazionale di Fisica Nucleare; the Ministry of Education, Culture, Sports, Science, and Technology of Japan; the Natural Sciences and Engineering Research Council of Canada; the National Science Council of the Republic of China; the Swiss National Science Foundation; the A. P. Sloan Foundation; the Bundesministerium fuer Bildung und Forschung, Germany; the Korea Science and Engineering Foundation (KoSEF); the Korea

TABLE I: Diphoton and dielectron limits on M_S in Hewett, GRW, and HLZ conventions. The final two rows show the combined limits with and without a K -factor.

		M_S^{95} (GeV/ c^2)							
Sample	K	Hewett		GRW	HLZ				
		$\lambda=-1$	$\lambda=+1$		$n=3$	$n=4$	$n=5$	$n=6$	$n=7$
CC $\gamma\gamma$		870	808						
CP $\gamma\gamma$		718	639						
CC+CP $\gamma\gamma$	1.0	899	797	1006	1197	1006	909	846	800
e^+e^-	1.0	780	768	873	1038	873	789	734	694
$e^+e^-+\gamma\gamma$	1.0	905	826	1013	1205	1013	916	852	806
$e^+e^-+\gamma\gamma$	1.3	939	853	1051	1250	1051	950	884	836

Research Foundation; and the Comision Interministerial de Ciencia y Tecnologia, Spain.

-
- [1] N. Arkani-Hamed, S. Dimopoulos, and G. Dvali, Phys. Lett. **B249**, 263 (1998).
[2] S. Murgia, Ph.D. Thesis, Michigan State University (2002).
[3] J. Carlson, Ph.D. Thesis, University of Michigan (2002).
[4] DØ Collaboration, B. Abbott *et al.*, Phys. Rev. Lett. **86**, 1156 (2001).
[5] K. Cheung and G. Landsberg, Phys. Rev. **D62**, 076003 (2000).
[6] F. Abe *et al.*, Nucl. Instrum. Methods, A **271**, 387 (1988).
[7] CDF Collaboration, T. Affolder *et al.*, Phys. Rev. **D64**, 092002 (2001).
[8] CDF Collaboration, F. Abe *et al.*, Phys. Rev. Lett. **79**, 2192 (1997).
[9] U. Baur, private communication.
[10] O. J. Eboli, T. Han, M. B. Magro and P. G. Mercadante, Phys. Rev. **D61**, 094007 (2000).
[11] H. Bengtsson and T. Sjöstrand, Comput. Phys. Commun. **46**, 43 (1987).
[12] CDF Collaboration, F. Abe *et al.*, Phys. Rev. Lett. **73**, 2662 (1994).
[13] J. Owens, private communication.
[14] CDF Collaboration, F. Abe *et al.*, Phys. Rev. **D50**, 2966 (1994).
[15] CTEQ Collaboration, H. L. Lai *et al.*, Eur. Phys. J. C **12**, 375 (2000) [arXiv:hep-ph/9903282].
[16] J. Hewett, Phys. Rev. Lett. **82**, 4765 (1999).
[17] G. F. Giudice, R. Rattazzi, and J. D. Wells, Nucl. Phys. **B544**, 3 (1999).
[18] T. Han, J. Lykken, and R. Zhang, Phys. Rev. **D59**, 105006 (1999).